Characterization of annealed *N,N′*-diphenyl-*N,N′*-di-p-tolylbenzene-1,4-diamine nanostructured thin films

Ahmed El-ghandour[1] · Abdou Eltamimy[3] · Mohamed Farhat O. Hameed[1,2,3] · S. S. A. Obayya[1,3]

Abstract

Exploring new efficient derivatives of polyphenylamines to act as a hole transport layer (HTL) in organic light emitting diodes is a global demand. Herein, we introduce *N,N′*-diphenyl-*N,N′*-di-p-tolylbenzene-1,4-diamine (NTD) as a potential HTL. Nanostructured films of NTD with thickness 75 nm are spin coated. Subsequently, these films are manipulated via annealing process and characterized using different techniques. The fluorescence spectrophotometer reveals that NTD film undergoes a Stokes shift of $3546\ cm^{-1}$ upon excition using a beam of wavelength of 365 nm. The X-ray diffraction analysis shows that NTD films consist of nanoparticles (NPs) with an average crystallite size of 33.43 nm. Upon annealing the films at temperatures of 373 and 423 K, the size of the NPs has climbed to 40.22 and 46.45 nm respectively. The UV/Vis spectroscopy indicates that the NTD films have transmittance values greater than 87% in the visible region, which are enough to meet the requirements of the HTL materials in optoelectronic devices. Additionally, the Urbach and bandgap energies are declined with the annealing temperatures. This is due to the dramatically ordering of the NTD NPs with the annealing process. Impedance spectroscopy is also conducted in the frequency range from 500 Hz to 5 MHz at temperatures of 303, 373, and 423 K. Further, the Nyquist plots (Z_{im} vs. Z_{re}) are fitted to an equivalent circuit using EC-Lab software. The impedance is descended by increasing the annealing temperature. On the same approach, the charge transfer resistance (R_{ct}) dropped from 69.61 to 23.27 kΩ when the temperature is risen from 303 to 423 K, which confirms the semiconductor behavior of the NTD films.

1 Introduction

Organic π-conjugated compounds that can transport charges (holes or electrons) efficiently deem necessary layers in organic light emitting diodes (OLEDs) and organic solar cells (OSCs) [1–3]. Particularly, the derivatives of conductive polymers such as polyphenylamines, polyacenes and polythiophenes, which are widely used as interfacial layers either as an electron transporting layer (ETL) or a hole transporting layer (HTL) [4–6].

Photogenerated charges are selectively extracted by the ETL and HTL from the photoactive layer. These charges are transported to the corresponding electrode within the OLED or the OSC devices. In such devices, electrons and holes must be injected at equal rate to achieve high efficiency. Otherwise, the surplus electrons will be recombined with holes, resulting in a lower operation efficiency [7]. The mobility of electrons and holes in the organic layer determines the efficiency of the device. For instance, in OLEDs, electrons are transported through the LUMO bands, while the holes are transferred through the HOMO bands [7].

The manipulation of the energy bandgap of the π-conjugated interfacial layers is a critical procedure for designing optoelectronic devices [8]. The conducting properties of an OSC are merely dependent on the energy gap, which is related to the electronic band structure and relies on the pressure and temperature [9]. The surface and

✉ Mohamed Farhat O. Hameed
mfarahat@zewailcity.edu.eg

✉ S. S. A. Obayya
sobayya@zewailcity.edu.eg

Ahmed El-ghandour
aelghandour@zewailcity.edu.eg

Abdou Eltamimy
abdoeltamimy@students.mans.edu.eg

1 Center for Photonics and Smart Materials, Zewail City of Science and Technology, October Gardens, 6th of October, Giza, Egypt

2 Nanotechnology Engineering Program, Zewail City of Science and Technology, October Gardens, 6th of October, Giza, Egypt

3 Faculty of Engineering, Mansoura University, Mansoura, Egypt

structural morphology of the thin film is highly dependent on the nucleation and grain growth process. Therefore, it is necessary to understand the surface morphology and growth mechanism of π-conjugated compounds in thin films for technical applications. The charge injection of organic semiconductor at the inorganic/organic, organic/organic or metal/organic interface can be improved by handling the morphology.

Annealing of the organic thin films may lead to an ordered orientational stacking of the molecules, which results in a grain growth along one particular orientation [10]. Further, an improvement in the degree of crystallinity can be achieved within the structure of the thin film [11]. The annealing process decreases the bandgap due to increased atomic vibrations with a larger average interatomic spacing. The correlation between induced changes in the structure (average crystallite size and microstrain) and optical properties of the π-conjugated molecules is a key factor for choosing organic materials for efficient OLEDs and OSCs.

Looking for novel HTLs for optoelectronic devices is very meaningful. The HTL transports holes within the HOMO level and electrons within the LUMO level to a lesser degree. Therefore, the HTL materials should possess low ionization potential and high hole mobility. In our previous work [12], we have demonstrated that the optical properties of N,N'-diphenyl-N,N'-di-p-tolylbenzene-1,4-diamine (NTD) thin films are thickness dependent. The thinnest film shows the highest absorption and the lowest energy bandgap with a great potential to serve as HTL in OLEDs. Herein, we pursue the reporting on the NTD nanostructured thin film with optimum thickness of 75 nm. Particularly, we will shed the light on the manipulation of the structural, optical properties and electrical impedance using a facile annealing process at different temperatures in the ambient atmosphere. Besides, the fluorescence analysis of the pristine films is addressed. It is believed that the current results alongside with the previous work [12] will give a clear image about the possibility of employing NTD molecules as a hole transport layer in OLEDs and OSCs.

2 Materials and methods

The NTD powder is purchased from Sigma–Aldrich and deposited without further purification. The optimized structure of NTD shown in Fig. 1 is defined using density function theory (DFT) method with employing 6-311G++(d,p) as a basis set. Thereafter, substrates of glass and quartz are cleaned by a typical procedure in an ultrasonic bath with DI water, ethanol and acetone for each of 15 min and dried with nitrogen gas. Subsequently, the NTD solution is spincoated via employing Laurel Spin Processor (WS-650Mz-23NPP). The fluorescence spectrophotometer (Model: 6285)
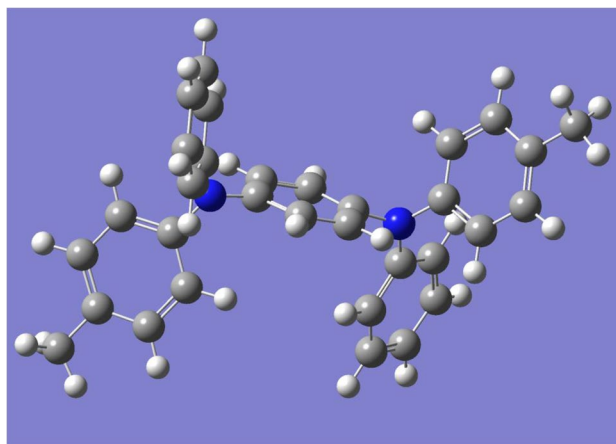

Fig. 1 Optimized structure of N,N'-diphenyl-N,N'-di-p-tolylbenzene-1,4-diamine (NTD). Color code: gray-carbon; blue-nitrogen; and white-hydrogen. (Color figure online)

is employed to examine the fluorescent properties of the NTD pristine film. A beam of wavelength 365 nm is used to excite the film in the cuvette. Both excitation and emission spectra are recorded. The pristine film (75 nm) is placed in a tubular furnace (MTI 1700×) for 30 min to undergo an annealing at 373 K and 423 K with heating rate of 10 °C/min. The crystal structure of the pristine and annealed NTD thin films is checked via X-ray diffraction technique (XRD) using Shimadzu XRD-6000 diffractometer. A radiation source of λ = 0.15408 nm belongs to Cu Kα is employed. Besides, the tube operation conditions are the scanning rate of 2°/min, and operating voltage of 50 kV with 40 mA current. The XRD patterns are recorded in the 2θ range from 4° to 90° at ambient temperature. The UV-visible-IR spectroscopy is conducted to measure the transmittance T (λ) and the reflectance R (λ) through a range of wavelengths from 250 to 2350 nm. The real and imaginary parts of the impedance are obtained in the frequency range from 500 Hz to 5 MHz at temperatures of 303, 373, and 423 K via employing RLC bridge (FLUKE PM6306).

3 Results and discussion

3.1 Fluorescence studies

Figure 2 shows the excitation/emission spectrum of the NTD thin film excited by a UV filter (365 nm). It is evident from this figure that a shift toward longer wavelengths is existed due to the Stokes Shift. Herein, the Stokes shift equals 3546 cm^{-1}. This quite large value of Stokes shift can be attributed to the difference between ground and excited state dipole moment. Moreover, it reveals a fast relaxation from the initial state to the emissive state due to intramolecular

**Fig. 2** Excitation and emission spectra of the NTD thin film
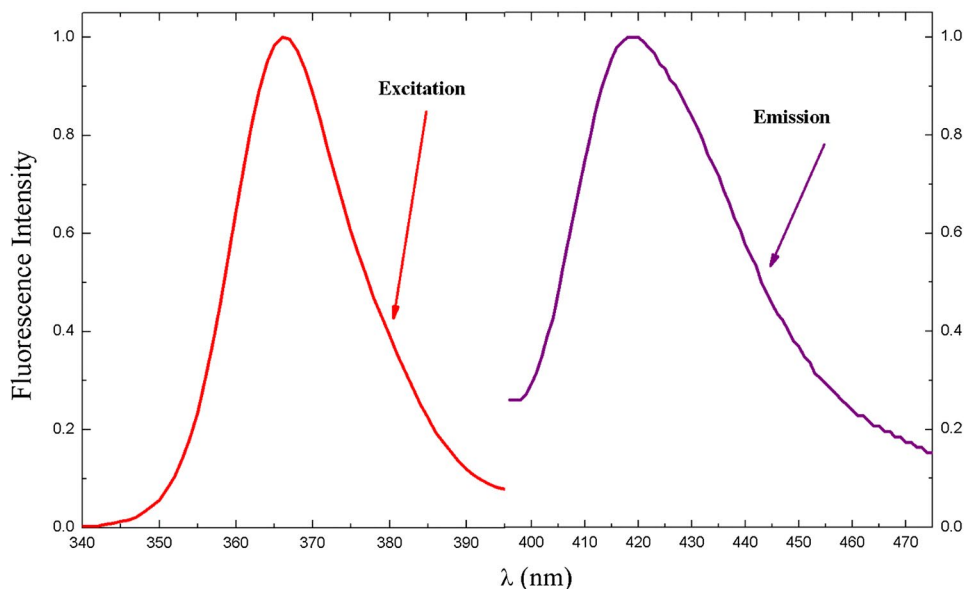
energy-transfer. In this context, part of the molecule can act as a donor to absorb the light while another portion of acts as an acceptor which emits light with a significant red shift.

3.2 Structure investigations

Figure 3 reveals the XRD patterns of the NTD thin films in the pristine as well as different annealed conditions. In general, the NTD films have a poly crystalline structure. The annealing temperatures enhance the crystallinity of the films with a growth of sharp broad peak at $2\theta = 31.85°$. Moreover, the diffraction peaks at $2\theta = 31.85°$ and $43.98°$ are indexed to the planes (112) and (201), respectively. These peaks can be assigned to the presence of methylenazo groups in the structure of the NTD thin films structure [13, 14]. The peaks profile of thin films usually arises due to the instrumental peak profile, crystallite size and the microstrain. Herein, these contributions are deconvoluted via employing Williamson–Hall (W–H) method to estimate the crystallite size and the microstrain [15]. The calculated values of the average

Fig. 3 The XRD patterns of the NTD films before and after annealing at T = 373 and 423 K
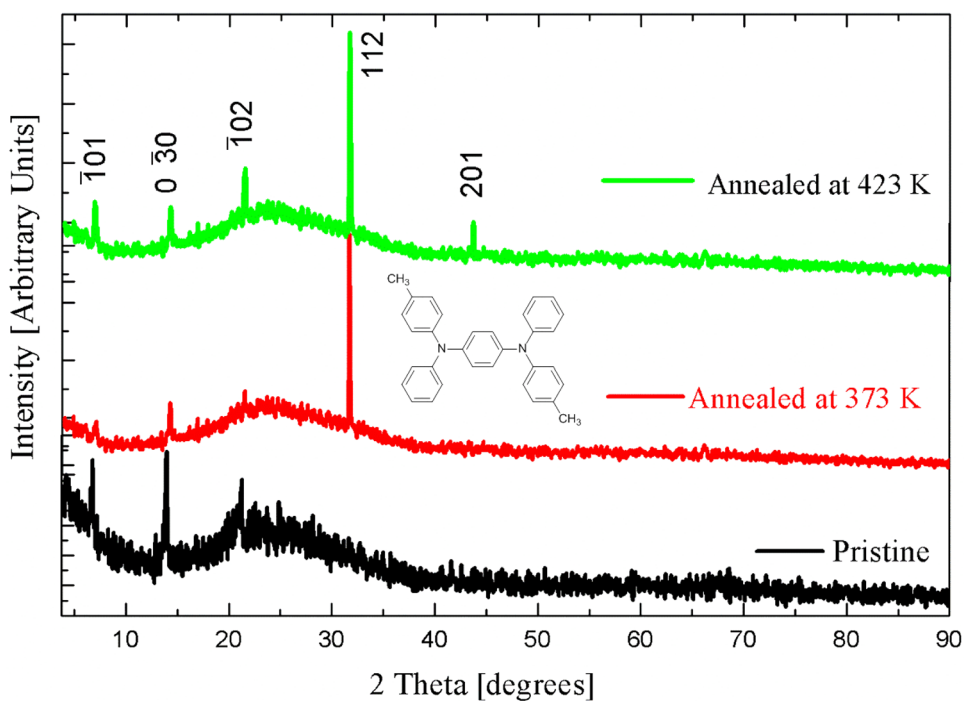
crystallite size and the microstrain are listed in Table 1. It is evident from this table that the pristine NTD film consists of nanoparticles (NPs) of average size 33.43 nm. Upon annealing the films at T = 373 and 423 K, the sizes of the NPs are increased to 40.22 and 46.45 nm, respectively. On contrary, the microstrain is decreased gradually with increasing the annealing temperature. For example, the microstrain of the annealed film at 423 K has been decreased by 37% in comparison to the fresh state.

3.3 Optical analysis

Figure 4 shows the normalized transmittance of the NTD films annealed at different temperatures. It is evident from this figure that the thin films are highly transparent with high

Table 1 Structural parameters, energy bandgaps, and Urbach energy of NTD films at different annealing conditions

Films annealing temperatures (K)	Optical bandgap E_g (eV)		Urbach energy E_e (eV)	Crystallite size D (nm)	Microstrain M ($\times 10^{-3}$)
	Direct	Indirect			
Pristine	3.05	2.56	1.02	33.43	9.05
373	2.95	2.39	0.83	40.22	7.41
423	2.75	2.16	0.78	46.45	5.77

NTD N,N′-diphenyl-N,N′-di-p-tolylbenzene-1,4-diamine

transmission greater than 85% with no intrinsic absorption. It is worth nothing that the opto-electronic devices based on optical waveguides require highly transparent thin films. In this context, the NTD films are a promising candidate for this purpose and other optoelectronic applications. The presence of identical intense peaks at 275 nm in the UV region is reasonably assigned to the jump from a nitrogen lone pair into a pi anti-bonding orbital, i.e., n → π* transition.

The film's surface morphology and roughness can control the incident light reflectance. The reflectance spectra of the pristine and annealed NTD thin films are presented in Fig. 5. From this figure, the pristine film reveals the highest percentage of reflectance. The surface reflectance decreases by 27% and 72% when the films are annealed at 373 and 423 K, respectively.

The absorption coefficient $\alpha(\nu)$ at a frequency ν can be directly deduced from the measured optical transmittance spectra using the relationship:

$$\alpha(\nu) = \frac{1}{d} \ln\left(\frac{1}{T}\right) \tag{1}$$

where T is the transmittance and d is the thickness of the film. The fundamental absorption edge is one of the most important traits of the absorption spectra of the crystalline and amorphous materials. This edge follows an exponential law:

Fig. 4 Normalized transmission spectra of the NTD films manipulated at different annealing temperatures. Inset: transmission values in the UV region
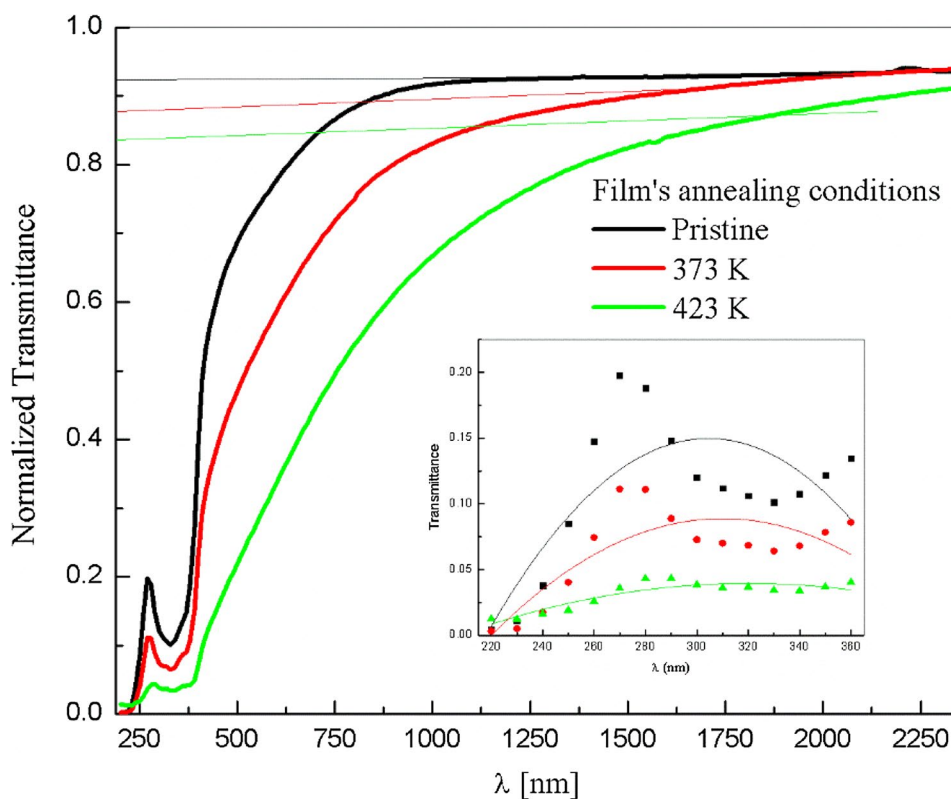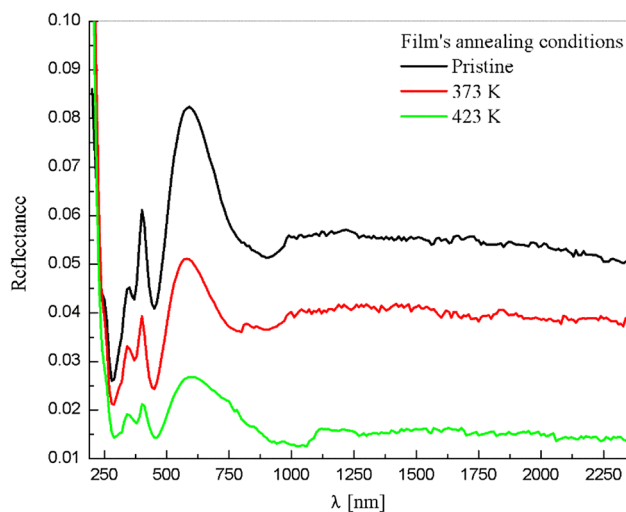
Fig. 5 Reflectance spectra of the NTD films treated at different annealing temperatures

$$\alpha h = B(h - E_g)^q \qquad (2)$$

where B is a constant, E_g is the optical energy gap and r is an index with values of 0.5, 1.5, 2 and 3, depending on the electronic transition type. Herein, the values of $r=2$ and r $= \frac{1}{2}$ represent the best fit of the experimental data which in turn propose the presence of the direct and indirect optical transition. The value of E_g is obtained from the plots of $(\alpha h\upsilon)^{1/2}$ and $(\alpha h\upsilon)^2$ in the high absorption range where the linear regions of the plots are extrapolated to zero absorption as shown in Fig. 6.

Table 1 illustrates that the direct and indirect energy bandgaps decrease on annealing, probably due to the segregation effects and crystallinity enhancement of the films as reported earlier on XRD investigations in Sect. 3.2 and

for other organic materials in [16, 17]. Tailoring devices of large internal quantum efficiencies require materials with low Urbach energy. The Urbach energy sheds the light on the disorder in the material. Besides, any change in the width of Urbach tail significantly affects the energy bandgap. Figure 7 illustrates the spectra of $ln\ (\alpha)$ versus the $h\upsilon$ for the pristine film of the NTD and the annealed films. The observed straight lines affirm the dependence of the absorption coefficient on the photon energy in accordance with the Urbach formula:

$$\alpha\upsilon = \alpha_o e^{\left(h\upsilon/E_e\right)} \qquad (3)$$

where α_o is a constant and E_e is an energy corresponding to the width of the tails of the localized states in the forbidden gap. The values of E_e are also listed in Table 1. It may be also observed from Table 1 that the values of E_e decline by increasing the annealing temperatures. It seems that the NTD nanostructured films get ordered together dramatically upon the annealing at 373 and 423 K which in turn decreases the Urbach energy and bandgaps.

3.4 Impedance spectroscopy

Electrochemical impedance spectroscopy (EIS) is also performed to study the electrical characteristics of the NTD film under dark conditions in the frequency range from 500 Hz to 5 MHz and at selected temperatures 303, 373, and 423K. The concept of impedance is usually conducted to address a quantitative representation of the opposition force to electrical current in the AC circuits [18]. The real and imaginary impedance parts are plotted against each other in Nyquist plots for the NTD films as depicted in Fig. 8. It is evident from this figure that when the temperature increases, the impedance decreases. This behavior
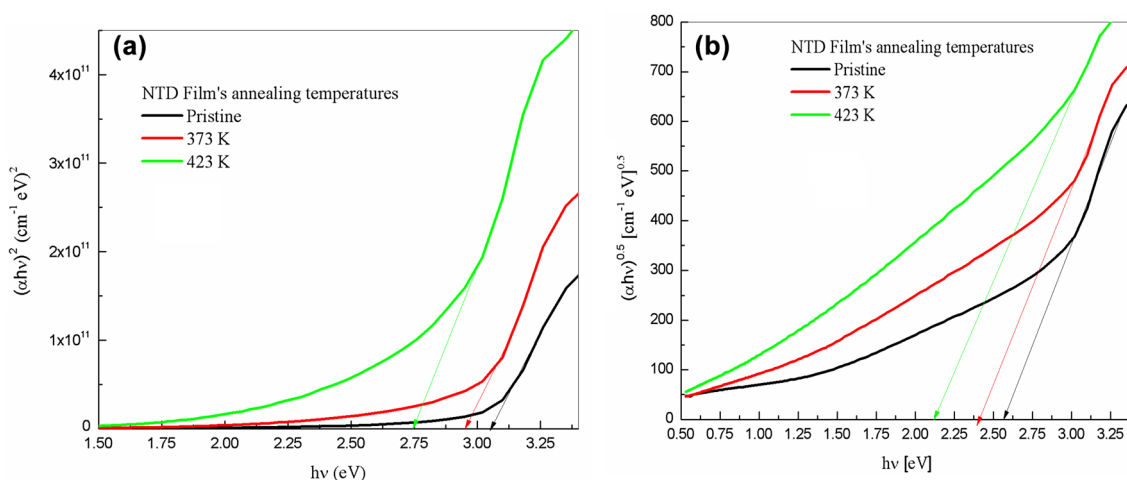

Fig. 6 Type of electronic transitions involved in the NTD thin films: **a** direct transitions and **b** indirect transitions
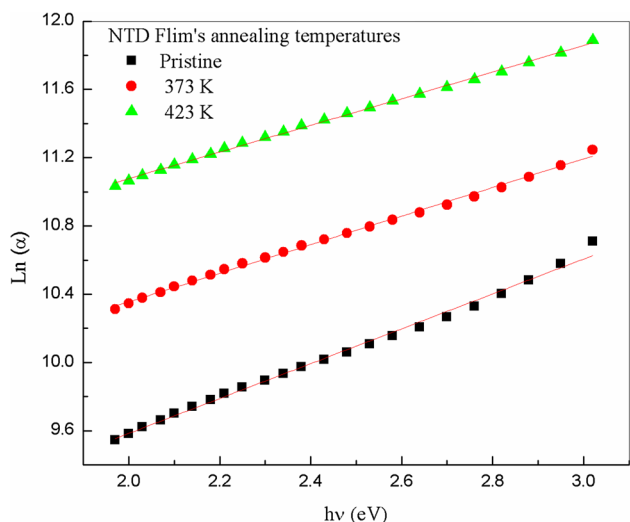
Fig. 7 Urbach tails of the NTD thin films at different annealing temperatures
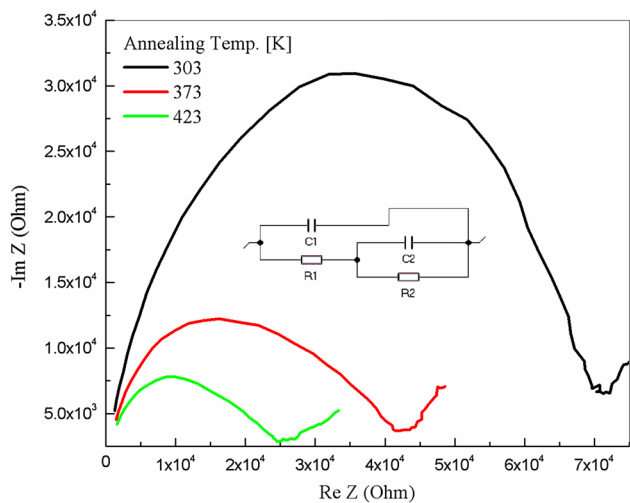

Fig. 8 Complex impedance at different temperatures and equivalent circuit mode of NTD films

is well documented for other organic materials [19]. The fittings of the curves are performed using the commercial software EC-Lab [20]. The impedance of the equivalent circuit illustrated in the inset of Fig. 8 and it is equal to:

$$Z(f) = \frac{R_2 + R_1(1 + i2\pi f C_2 R_2)}{1 + i2\pi f C_2 R_2 + i2\pi f C_1((R_2 + R_1(1 + i2\pi f C_2 R_2)))} \quad (4)$$

The extracted parameters of the elements in the two equivalent circuits are summarized and listed in Table 2. This table indicates that the charge transfer resistance (R_{ct}) decreases gradually with elevating the temperature, which means that

Table 2 Extracted parameters for the circuit elements at different temperatures

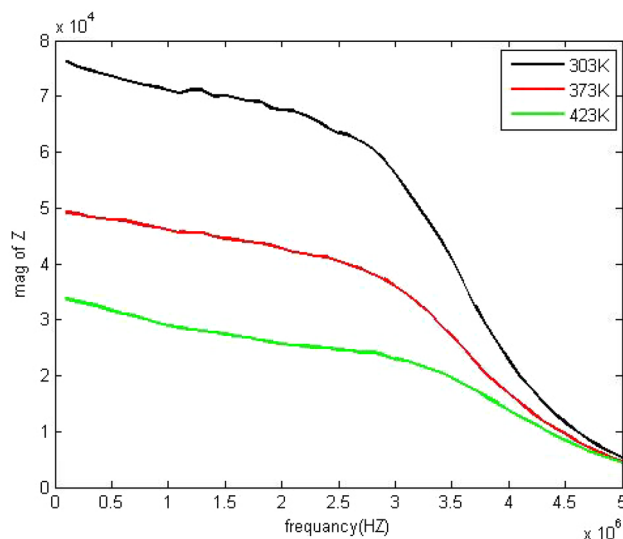| T (K)	C_1 (µF)	R_1 (Ω)	C_2 (µF)	R_2 (Ω)	R_{ct} (kΩ)
303	1.05	15,556	1.955	8356	69.61
373	0.692	16,845	44.85	22.36×10^{-6}	40.35
423	0.955	13,438	12.84×10^{-6}	2955	23.27

Fig. 9 Bode plots of NTD film at different annealing temperatures

the opposition experienced to the electron movements are less considerable after the annealing process.

It should be noted that the NTD film sandwiched between two electrodes represents an electrochemical cell, which can be modeled as a network of passive electrical circuit elements. The relations between R_1, R_2, C_1, C_2 and the NTD film can be interpreted by plotting the Bode plot as depicted in Fig. 9. It may be seen from this figure that the impedance of C_1 and C_2 tends to zero values at high frequency based on the relation:

$$Z_C(f) = \frac{1}{j2\pi f C} \quad (5)$$

However, the impedance of C_1 and C_2 soar by decreasing the frequency. Therefore, the equivalent circuit reveals that the net impedance of the film at low frequency is equal to $Z_{net} = R_2 + R_1$. While at high frequency, the net impedance of the studied file tends to zero $Z_{net} = 0$. As a result, the NTD film can act as a high transimpedance at low frequencies (DC) with intrinsic gain of ($R_2 + R_1$).

Table 3 illustrates the performance of the reported HTL (NTD) relative to other HTLs in the literature to clarify the advantage of the present work over the preceding ones. It is evident from this table that the thermal gravimetric

Table 3 Comparison between physical, chemical, thermal and optical properties of previously reported HTL materials in the literature and the suggested NTD

Abbrev.	Full form	Formula	Mol. wt (g/mol)	TGA (°C)	Absorption λ (nm)	Emission λ (nm)	Ref.
NTD	N,N'-diphenyl-N,N'-di-p-tolylbenzene-1,4-diamine	$C_{32}H_{28}N_2$	440.58	270	365	420	Present work
TPD	$N,N0$ -bis(3-methyl phenyl)-$N,N0$ -bis(phenyl)-benzidine	$C_{38}H_{32}N_2$	516.67	300	352 (in THF)	398 (in THF)	[21]
α-NPD	$N,N0$ -bis(naphthalen-1-yl)-$N,N0$ -bis(phenyl)-2,20—dimethylbenzidine	$C_{46}H_{36}N_2$	616.79	310	307 (in CH_2Cl_2)	447 (in CH_2Cl_2)	[7]
Spiro-NPB	$N,N0$ -bis (naphthalen-1-yl)-$N,N0$ -bis(phenyl)-9,9-spirobifluorene	$C_{57}H_{38}N_2$	750.93	390	380 (in THF)	453 (in THF)	[22]
Spiro-TPD	$N,N0$ -bis(3-methylphenyl)-$N,N0$ -bis(phenyl)-9,9-spirobifluorene	$C_{51}H_{38}N_2$	678.86	280	379 (in THF)	416 (in THF)	[23]

analysis (TGA) of the reported NTD guarantees a stable morphology under operation conditions of OLEDs and solar cells. Further, as the excitation wavelength (365 nm) of the NTD films is below the visible region, NTD will not absorb the incident light. Therefore, the NTD layer can be used in improving solar cell efficiency. In the same context, the emission wavelength of the NTD films in the visible region (420 nm) fits the requirements of OLEDs and other optoelectronic device based on the fluorescence phenomena.

4 Conclusion

The characteristics of N,N'-diphenyl-N,N'-di-p-tolylbenzene-1,4-diamine nanostructured thin films are studied and discussed. It has been shown that the electronic functionality of the NTD molecules as a hole transport layer is maintained where the crystallinity of the films is significantly improved upon the annealing process. The surface reflectance decreases by 27% and 72% when the films are annealed at 373 and 423 K, respectively. The fluorescence activity of the NTD films is existed with quite large Stokes shift (3546 cm^{-1}) which ensures that the suggested material can act as HTL in OLEDs. Additionally, the facile annealing has induced the energy bandgap significantly, which facilitates the charge carriers' movement from the localized states to the delocalized states. Further, the values of Urbach energy E_e decrease on increasing annealing temperatures owing to the induced ordering of the NTD molecules upon annealing. These results agree well with the XRD analysis of the prepared samples. Further, the charge transfer resistance is decreased from 69.61 kΩ at room temperature to 40.35 and 23.27 kΩ when the films annealled at 373 and 423 K, respectively.

References

1. X. Zhao, X. Zhan, Chem. Soc. Rev. **40**, 3728 (2011)
2. D.M. De Leeuw, E. Cantatore, Mater. Sci. Semicond. Process. **11**, 199 (2008)
3. V. Coropceanu, J. Cornil, D.A. da Silva Filho, Y. Olivier, R. Silbey, J.-L. Brédas, Chem. Rev. **107**, 926 (2007)
4. X. Yang, L. Wang, C. Wang, W. Long, Z. Shuai, Chem. Mater. **20**, 3205 (2008)
5. Y. Shirota, J. Mater. Chem. **10**, 1 (2000)
6. J.E. Norton, K.N. Houk, J. Am. Chem. Soc. **127**, 4162 (2005)
7. N.T. Kalyani, S.J. Dhoble, Renew. Sustain. Energy Rev. **44**, 319 (2015)
8. M. Grätzel, Inorg. Chem. **44**, 6841 (2005)
9. Y. Noguchi, A. Saeki, T. Fujiwara, S. Yamanaka, M. Kumano, T. Sakurai, N. Matsuyama, M. Nakano, N. Hirao, Y. Ohishi, S. Seki, J. Phys. Chem. B **119**, 7219 (2015)
10. D. Roy, N.M. Das, P.S. Gupta, AIP Adv. **80**, 42514–42522 (2014)
11. M.M. El-Nahass, H.M. Zeyada, N.A. El-Ghamaz, A.E.-G. Shetiwy, Optik (Stuttg). **171**, 580 (2018)
12. A. El-ghandour, M.F.O. Hameed, A.S. Awed, S.S.A. Obayya, Appl. Phys. A **124**, 543 (2018)
13. B.G.R. Agarwal, M.S. Alam, J. Appl. Polym. Sci. **129**, 3728 (2013)
14. A.F. Al-Hossainy, M.S. Zoromba, J. Mol. Struct. **1156**, 83 (2018)
15. B. York, in *New X-Ray Diffr. Line Profile Funct. Based Cryst. Size Strain Distrib. Determ. from Mean F. Theory Stat. Mech.* (MIT Center for Materials Science and Engineering, 1997), p. 41
16. E. Çetinörgü, S. Goldsmith, Y. Rosenberg, R.L. Boxman, J. Non-Cryst. Solids **353**, 2595 (2007)
17. A. El-ghandour, A.S. Awed, M.M.A.-E. khier, K. Abdeen, M.I.A. El Maaty, Opt. Laser Technol. **112**, 126 (2019)
18. E.P. Randviir, C.E. Banks, Anal. Methods **5**, 1098 (2013)

19. M.A. Fersi, I. Chaabane, M. Gargouri, Phys. E Low-Dimens. Syst. Nanostruct. **83**, 306 (2016)
20. EC-Lab® software V11.10 (2011)
21. L.C. Palilis, H. Murata, M. Uchida, Z.H. Kafafi, Org. Electron. **4**, 113 (2003)
22. J.C.S. Costa, R.J.S. Taveira, C.F.R.A.C. Lima, A. Mendes, L.M. Santos, Opt. Mater. (Amst). **58**, 51 (2016)
23. J. Kirkpatrick, J. Nelson, J. Chem. Phys. **123**, 084703 (2005)